

Suppressed Magnetization in $\text{La}_{0.7}\text{Ca}_{0.3}\text{MnO}_3/\text{YBa}_2\text{Cu}_3\text{O}_{7-\delta}$ Superlattices

A. Hoffmann* and S. G. E. te Velthuis

Materials Science Division, Argonne National Laboratory, Argonne, Illinois 60439

Z. Sefrioui and J. Santamaría

GFMC. Dpto. Física Aplicada III,

Universidad Complutense de Madrid, 28040 Madrid, Spain

M. R. Fitzsimmons and S. Park

Los Alamos National Laboratory Los Alamos, New Mexico 87545

M. Varela

Condensed Matter Sciences Division,

Oak Ridge National Laboratory, Oak Ridge, Tennessee 37831-6030

(Dated: March 24, 2018)

Abstract

We studied the magnetic properties of $\text{La}_{0.7}\text{Ca}_{0.3}\text{MnO}_3 / \text{YBa}_2\text{Cu}_3\text{O}_{7-\delta}$ superlattices. Magnetometry showed that with increasing $\text{YBa}_2\text{Cu}_3\text{O}_{7-\delta}$ layer thickness the saturation magnetization per $\text{La}_{0.7}\text{Ca}_{0.3}\text{MnO}_3$ layer decreases. From polarized neutron reflectometry we determined that this magnetization reduction is due to an inhomogeneous magnetization depth profile arising from the suppression of magnetization near the $\text{La}_{0.7}\text{Ca}_{0.3}\text{MnO}_3 / \text{YBa}_2\text{Cu}_3\text{O}_{7-\delta}$ interface. Electron energy loss spectroscopy indicates an increased 3d band occupation of the Mn atoms in the $\text{La}_{0.7}\text{Ca}_{0.3}\text{MnO}_3$ layers at the interface. Thus, the suppression of ferromagnetic order at the $\text{La}_{0.7}\text{Ca}_{0.3}\text{MnO}_3 / \text{YBa}_2\text{Cu}_3\text{O}_{7-\delta}$ interface is most likely due to charge transfer between the two materials.

PACS numbers: 74.45.+c, 74.78.Fk, 75.70.Cn

The interplay between ferromagnetism and superconductivity has been of longstanding research interest, since the competition between these generally mutually exclusive types of long-range order gives rise to a rich variety of phenomena.¹ Using ferromagnetic (F)/superconducting (S) layered heterostructures enables investigation of diverse effects, i.e., non-monotonic changes of the superconducting transition temperature² T_c and π -Junctions³ in S/F/S structures, and the dependence of T_c on the relative magnetization direction in F/S/F structures.⁴ Layered heterostructures also offer opportunities to help resolve theoretical predictions with respect to F/S structures, such as triplet superconductivity.⁵

Most studies of F/S heterostructures involved transition metal systems. But there is increasing interest in F/S structures in which combinations of complex materials based on perovskite oxides are used, since these materials on their own show unusual properties. Many different cuprate high- T_c superconductors are characterized by a short superconducting coherence length and an anisotropic superconducting gap. At the same time manganites are atypical ferromagnets in that they exhibit colossal magnetoresistance and are potentially half-metallic. Since both classes of materials have very similar perovskite structures with comparable lattice constants in the basal plane, it is possible to combine them into structurally coherent superlattices with very sharp interfaces.^{6,7} Previous experiments have already shown that cuprate/manganite based superlattices have distinctively different properties compared to their transition metal counterparts. They exhibit unusually long ranging proximity effects,⁸ spin injection into the superconducting layer,⁹ and even giant magnetoresistance.¹⁰

Previous work mostly focused on the influence of proximity effects on the superconducting properties like the superconducting transition temperature or critical current density. Here, we focus on the magnetic properties of the magnetic layers. In this paper we show that in $\text{La}_{0.7}\text{Ca}_{0.3}\text{MnO}_3$ (LCMO) / $\text{YBa}_2\text{Cu}_3\text{O}_{7-\delta}$ (YBCO) superlattices the ferromagnetic ordering is suppressed at the interface between LCMO and YBCO. This adds more complexity for explaining proximity effects in oxide based heterostructures.

The LCMO/YBCO superlattices were grown by high pressure sputtering on (100) SrTiO_3 substrates. For one series of superlattices the LCMO layer thickness was kept constant at 15 unit cells (corresponding to 60 Å), while the YBCO layer thickness was varied between 1 and 12 unit cells. X-ray diffraction indicated that the samples are epitaxial and x-ray reflectivity showed that the interfaces are well defined with roughnesses below one unit cell

for the layers close to the substrate. The roughness increased to about 35 Å for the top-most layers. Scanning transmission electron microscopy also indicated a similar trend for the interface roughnesses. Magnetic hysteresis loops were measured with a Quantum Design superconducting quantum interference device system. Polarized neutron reflectometry measurements were taken on $5 \times 10 \text{ mm}^2$ samples using POSY1 at IPNS (Argonne) and ASTERIX at LANSCE (Los Alamos). Electron microscopy observations and electron energy loss spectroscopy (EELS) measurements were obtained in a dedicated scanning transmission scanning microscope VG Microscopes HB501UX, operated at 100 kV and equipped with a Nion aberration corrector and an Enfina EEL spectrometer. Cross sectional specimens were prepared by conventional methods: grinding, dimpling, and Ar ion milling at 5 kV. Final cleaning was performed at 0.5 kV.

The saturation magnetization attributed to the LCMO layers shows a drastic reduction with decreasing LCMO thickness (Fig. 1). The saturation magnetization is well below both the bulk value¹¹ of $M_s = 576 \text{ emu/cm}^3$ and the values of $M_s \approx 400 \text{ emu/cm}^3$ observed for single layer LCMO thin films¹² prepared under similar conditions as the superlattices discussed in this paper. Previously, the saturation magnetization of YBCO/LCMO superlattices were observed to achieve values comparable to single layer LCMO films only when the LCMO layer thickness exceeded 100 unit cells¹³ (in our case the thickness is 15 unit cells). This observation implies that the proximity of YBCO to LCMO affects the magnetic properties of LCMO for either intrinsic or extrinsic reasons.

An important key to understanding the origin of the reduced magnetization in the LCMO can be found in the magnetization depth profile of each LCMO layer. This information can be readily obtained from polarized neutron reflectometry.¹⁴ Briefly, the technique involves reflection of a polarized neutron beam with wave vector \mathbf{k}_i from the sample onto a polarization analyzer with wave vector \mathbf{k}_f . Use of a polarized beam with polarization analysis permits determination of the spin-dependent neutron reflectivities. The difference between the non-spin-flip reflectivities R^{++} and R^{--} (with the neutron spin parallel and antiparallel to the applied field, respectively) is determined by the component of the magnetization depth profile, which is parallel to the applied magnetic field and perpendicular to $\mathbf{q} = \mathbf{k}_f - \mathbf{k}_i$. In our experiment the magnetic field is applied along the surface plane. Since we performed our measurements in saturation (as determined by magnetometry), the perpendicular magnetization component is zero and we only present non-spin-flip reflectiv-

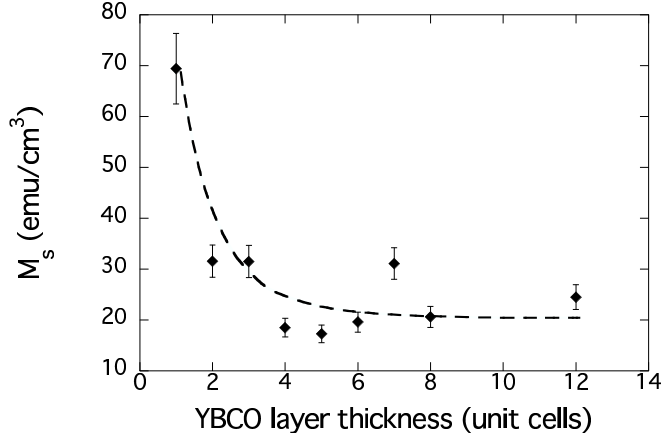


FIG. 1: Saturation magnetization measured at 100 K normalized to the LCMO volume for [LCMO 15 u.c./YBCO n u.c.] superlattices with varying YBCO thickness. The dashed line is a guide to the eye.

ities. The momentum transfer (q -dependence) of the reflectivities is related to the Fourier components of the magnetization depth profile – providing depth sensitivity.¹⁵ Using an iterative process,¹⁶ the reflectivities calculated from model structures comprised of chemical and magnetical depth profiles, can be fitted to the observed reflectivities.

Figure 2 shows polarized neutron reflectivities for a sample with 3 unit cell thick YBCO layers. The measurements were taken with the sample at 120 K and an applied field of 5.4 kOe. The first and second Bragg peaks due to the superlattice structure are clearly visible. In order to analyze the neutron reflectivity data we first determined the chemical structure with X-ray reflectivity, which is shown with the corresponding fit in the inset of Fig. 2. The structural parameters were then used for the subsequent fit of the neutron reflectivity data, where the only free parameters were the neutron scattering length densities and the magnetization depth profile.

For the fit of the polarized neutron reflectivity data we used two different models for the magnetization depth profile. One where the magnetization is homogeneous throughout each LCMO layer, and the other in which the magnetization is inhomogeneous such that the magnetization is suppressed close to the LCMO/YBCO interface. For comparison of the two cases, we plot in Fig. 3 the measured neutron spin asymmetry $(R^{++} - R^{--})/(R^{++} + R^{--})$ together with the best fits for both the homogeneous and the inhomogeneous model. Notice, that the sign of the spin asymmetry is opposite for the two model calculations

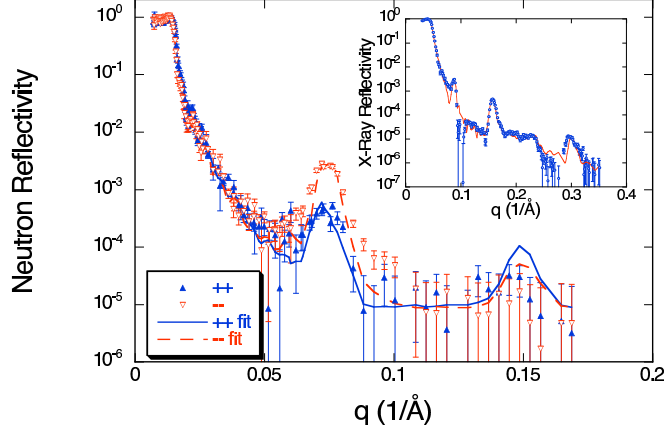


FIG. 2: (Color online) Polarized neutron reflectivity for the [LCMO 15 u.c./YBCO 3 u.c.] superlattice in saturation. The inset shows X-ray reflectivity for the same sample. The experimental data is presented by the symbols, while the lines are fits. The fit for the neutron data is based on the model using an inhomogeneous magnetization as discussed in the text.

at the position of the second superlattice Bragg peak (at 0.15 1/\AA). The sign of the spin asymmetry is positive for the inhomogeneous case, while it is negative for the homogeneous case. Experimentally the asymmetry integrated around the second superlattice peak ($q = 0.13\text{--}0.17 \text{ 1/\AA}$) is clearly positive: $A = 0.4 \pm 0.3$. This shows unambiguously that the magnetization in the LCMO is reduced close to the interface with YBCO. In addition the experimental spin asymmetry near the critical edge and first superlattice Bragg peak is significantly better fitted by the inhomogeneous model. A direct comparison between the experimental polarized neutron reflectivities and the fits based on the inhomogeneous model is also shown in Fig. 2. An even better fit for the neutron data could be obtained if the structural parameters were also varied.

Recently, Stahn *et al.* explained their neutron reflectometry data with two possible scenarios; one with a suppressed magnetization in the LCMO, similar to our case, and the other one where close to the interface a net magnetic moment is induced in the YBCO layer, which should be antiparallel to the LCMO moments.¹⁷ We can exclude the latter possibility, since in our measurements, the reversal in sign of the spin asymmetry around the second Bragg peak is a smoking gun for the suppressed magnetization. We can exclude an additionally induced net magnetization in the YBCO, either parallel or antiparallel to the magnetization in the LCMO. Simulations for both cases always result in the wrong sign of

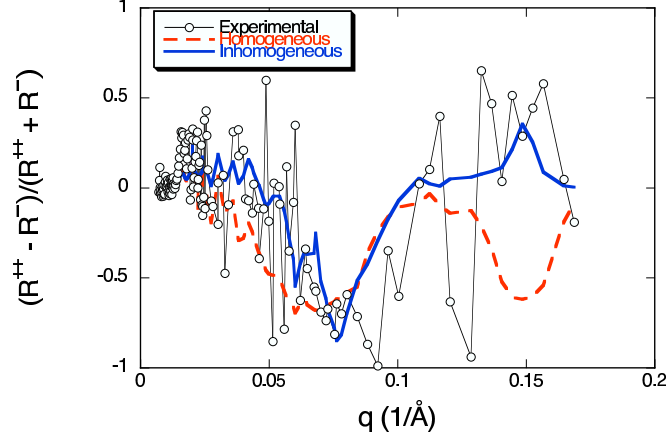


FIG. 3: (Color online) Spin asymmetry $(R^{++} - R^{--})/(R^{++} + R^{--})$ of the neutron reflectivity. The line with symbols indicate the experimental data, while the dashed and solid line indicate the fitted spin asymmetry for the homogeneous and inhomogeneous models, respectively.

the spin asymmetry at the second Bragg peak, similar to the homogenous model discussed previously.

The structural profile obtained from the fit to the X-ray data, and the magnetization profile obtained from the fit to the neutron data are shown in detail in Fig. 4(a). The magnetic layer thickness is reduced compared to the structural layer thickness over a distance up to $12 \pm 1 \text{ \AA}$ away from the interface into the LCMO. Furthermore, the magnetization in the middle of each LCMO layer ($158 \pm 7 \text{ emu/cm}^3$) is only about 1/3 of the bulk LCMO magnetization value. This reduced value may be partly due to the elevated temperature of the measurement and partly due to a charge transfer between the YBCO and the LCMO layer as discussed below.

In order to further investigate the origin of the reduced magnetization we performed EELS spectroscopy with atomic resolution. From the analysis of the Mn L edge at 640 eV the formal oxidation state of Mn in the LCMO can be determined.^{18,19} Figure 4(b) shows the variation of the Mn 3d band occupations across a single LCMO layer in a [LCMO 40 u.c./YBCO 12 u.c.] superlattice. These measurements were averaged over a lateral distance parallel to the interface of 6 nm. Based on the chosen chemical doping of the LCMO we anticipate 3.67 3d electrons per Mn ion, which is in good agreement with the occupation 3.62 ± 0.18 measured by EELS averaged over the whole LCMO layer. However, near the YBCO/LCMO interface a spatially inhomogeneous distribution was found. The number

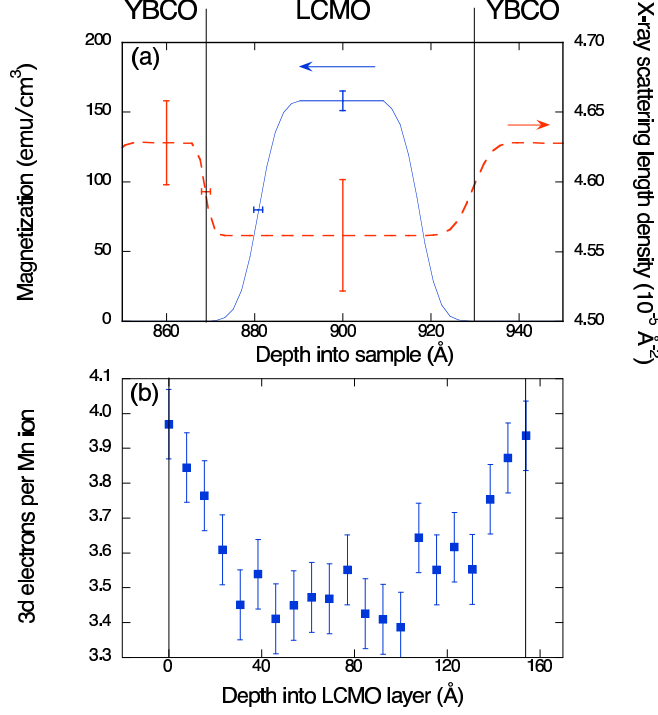


FIG. 4: (Color online) (a) Depth profile of the magnetization (from polarized neutron reflectometry) and chemical structure given by the X-ray scattering length density for the [LCMO 15 u.c./YBCO 3 u.c.] superlattice. The vertical lines indicate the structural LCMO/YBCO interfaces. Error bars for the model parameters of the fit are also indicated. (b) Occupation of the Mn 3d band as determined from EELS spectroscopy as a function of distance across one LCMO layer for a [LCMO 40 u.c./YBCO 12 u.c.] superlattice.

of 3d electrons per formula unit was found to increase, and the increase scaled inversely with the magnetization suppression. Interestingly, for close to four 3d electrons per Mn ion LCMO exhibits antiferromagnetic ordering. Also, the EELS data show an overall decrease in the number of 3d electrons per Mn ion in the center of the layer. A survey of other similarly prepared samples also found a general decrease of the electron occupation near the film center.²⁰ This suggests that there is a net charge transfer from the YBCO to the LCMO layer. Recently infrared absorption also found a long-range charge transfer in YBCO/LCMO superlattices.²¹

It is useful to estimate in the LCMO layer the Thomas-Fermi screening length $\lambda_{TF} = 1/2\sqrt{a_0/n^{1/3}}$, which is the typical length scale for charge inhomogeneities. Here a_0 is the Bohr radius and n is the charge carrier density, which in manganites is typically 10^{19} –

10^{22} cm^{-3} .²² Using this range of charge carrier density, we obtain $\lambda_{TF} = 2\text{--}6 \text{ \AA}$, which corresponds to a distance of one to two unit cells of the LCMO layers. From the fit to the neutron data we obtain a $12 \pm 1 \text{ \AA}$ thick region over which the magnetization is suppressed within each LCMO layer. The similarity of these length scales suggests that the suppression of the saturation magnetization may be due to a charge transfer across the interface. Also notice that band bending at the interface might give rise to a longer distance for charge redistributions than estimated by λ_{TF} . The continuously varying doping, as evidenced from the EELS measurements, may give rise to antiferromagnetic order close to the YBCO/LCMO interface, which again is consistent with the suppressed magnetization at the interface. The LCMO recovers ferromagnetic order only once it is further away from the interface. This interpretation of the data is also consistent with the recently observed exchange bias in YBCO/LCMO superlattices arising from exchange coupling between a ferromagnet and an antiferromagnet.^{23,24}

The depressed magnetization at the interface may also provide an explanation for the long range proximity effect reported recently in YBCO/LCMO heterostructures. Measurements of T_c of F/S/F trilayers and superlattices as a function of the thickness of the F layer suggest that the order parameter penetrates distances up to 5 nm into the ferromagnet.⁸ There should not be any ferromagnetic / (singlet) superconducting proximity effect if the LCMO were half metallic.²⁵ However, the suppressed magnetization at the interface and the depressed magnetization value within the LCMO layer suggest otherwise. The exchange splitting ΔE_{ex} is connected to the magnetic moment (μ) through an effective exchange integral I_{eff} as $\Delta E_{ex} = \mu I_{eff}$. The reduced moment may be reflecting a decreased exchange splitting thus providing a scenario for the penetration of the superconductivity into the ferromagnet.²⁶

In conclusion, we have shown unambiguously that the magnetization in LCMO layers is suppressed at the interface with YBCO. The suppression of magnetization at the interface is correlated with an increased occupancy of electron charge at the Mn sites. This suppression of magnetization may be a consequence of the redistribution of electric charges at the LCMO/YBCO interface.

We would like to acknowledge stimulating discussions with H.-U. Habermeier and J. Chakalian. This work was funded by MCYT MAT 2002-2642, Fundación Ramón Areces, CAM GR-MAT-0771/2004, and by the U. S. DOE, BES under contracts W-31-109-ENG-38,

- * Electronic address: hoffmann@anl.gov
- ¹ C. L. Chien and D. H. Reich, *J. Magn. Magn. Mater.* **200**, 83 (1999).
 - ² J. S. Jiang, D. Davidovic, D. H. Reich, and C. L. Chien, *Phys. Rev. Lett.* **74**, 314 (1995).
 - ³ V. V. Ryazanov, V. A. Oboznov, A. Y. Rusanov, A. V. Veretennikov, A. A. Golubov, and J. Aarts, *Phys. Rev. Lett.* **86**, 2427 (2001).
 - ⁴ J. Y. Gu, C.-Y. You, J. S. Jiang, J. Pearson, Y. B. Bazaliy, and S. D. Bader, *Phys. Rev. Lett.* **89**, 267001 (2002).
 - ⁵ A. F. Volkov, F. S. Bergeret, and K. B. Efetov, *Phys. Rev. Lett.* **90**, 117006 (2003).
 - ⁶ P. Prieto, et al., *J. Appl. Phys.* **89**, 8026 (2001).
 - ⁷ H.-U. Habermeier, G. Cristiani, R. K. Kremer, O. Lebedev, and G. van Tendeloo, *Physica C* **364**, 298 (2001).
 - ⁸ V. Peña, Z. Sefrioui, D. Arias, C. Leon, J. Santamaria, M. Varela, S. J. Pennycook, and J. L. Martinez, *Phys. Rev. B* **69**, 224502 (2004).
 - ⁹ S. Soltan, J. Albrecht, and H.-U. Habermeier, *Phys. Rev. B* **70**, 144517 (2004).
 - ¹⁰ V. Peña, Z. Sefrioui, D. Arias, C. Leon, J. Santamaria, J. L. Martinez, S. G. E. te Velthuis, and A. Hoffmann, *Phys. Rev. Lett.* **94**, 057002 (2005).
 - ¹¹ J. M. Coey, M. Viret, and S. von Molnár, *Adv. Phys.* **48**, 167 (1999).
 - ¹² G. Campillo, A. Berger, J. Osorio, J. E. Pearson, S. D. Berger, E. Baca, and P. Prieto, *J. Magn. Magn. Mater.* **237**, 61 (2001).
 - ¹³ Z. Sefrioui, D. Arias, V. Peña, J. E. Villegas, M. Varela, P. Prieto, C. León, J. L. Martinez, and J. Santamaria, *Phys. Rev. B* **67**, 214511 (2003).
 - ¹⁴ M. R. Fitzsimmons, et al., *J. Magn. Magn. Mater.* **271**, 103 (2004).
 - ¹⁵ M. R. Fitzsimmons and C. F. Majkrzak, in *Modern Techniques for Characterizing Magnetic Materials*, edited by Y. Zhu (Springer, New York, 2005), chap. 3, pp. 107–155.
 - ¹⁶ L. G. Parratt, *Phys. Rev.* **95**, 359 (1954).
 - ¹⁷ J. Stahn, et al., *Phys. Rev. B* **71**, 140509(R) (2005).
 - ¹⁸ H. Kurata and C. Colliex, *Phys. Rev. B* **48**, 2102 (1993).
 - ¹⁹ J. H. Rask, B. A. Miner, and P. R. Buseck, *Ultramicroscopy* **21**, 321 (1987).

- ²⁰ M. Varela, A. R. Lupini, V. Peña, Z. Sefrioui, I. Arslan, N. D. Browning, J. Santamaria, and S. J. Pennycook, *cond-mat/0508564*.
- ²¹ T. Holden, et al., *Phys. Rev. B* **69**, 064505 (2004).
- ²² C. H. Ahn, J.-M. Triscone, and J. Mannhart, *Nature (London)* **424**, 1015 (2003).
- ²³ N. Haberkorn, J. Guimpel, M. Sirena, L. B. Steren, W. Saldarriaga, E. Baca, and M. E. Gómez, *Appl. Phys. Lett.* **84**, 3927 (2004).
- ²⁴ P. Przyslupski, I. Komissarov, W. Paszkowicz, P. Dluzewski, R. Minikayev, and M. Sawicki, *Phys. Rev. B* **69**, 134428 (2004).
- ²⁵ M. J. M. de Jong and C. W. J. Beenakker, *Phys. Rev. Lett.* **74**, 1657 (1995).
- ²⁶ J. Aarts, J. M. E. Geers, E. Brück, A. A. Golubov, and R. Coehoorn, *Phys. Rev. B* **56**, 2779 (1997).